COMPUTATIONAL FLUID DYNAMICS MODELLING OF FLOCCULATION IN WATER TREATMENT: A REVIEW

J. Bridgeman*, B. Jefferson** and S. A. Parsons**

*School of Engineering (Civil Engineering), University of Birmingham, Edgbaston, Birmingham, B15 2TT, UK
E-Mail: j.bridgeman@bham.ac.uk (Corresponding Author)
** Centre for Water Science, School of Applied Sciences, Cranfield University, Cranfield, Bedfordshire, MK43 0AL, UK

ABSTRACT: The principal focus of this paper is to present a critical review of current approaches to modelling the inter-related hydrodynamic, physical and chemical processes involved in the flocculation of water using Computational Fluid Dynamics (CFD). The flows inside both laboratory and full scale mechanically-mixed flocculators are complex and pose significant challenges to modellers. There exists a body of published work which considers the bulk flow patterns, primarily at laboratory scale. However, there is little reported multiphase modelling at either scale. Two-equation turbulence modelling has been found to produce variable results in comparison with experimental data, due to the anisotropic nature of the swirling flow. However, the computational expense of combining the sliding mesh treatment for a rotating mesh with the Reynolds Stress Model (RSM) in a full scale unit is great, even when using a high performance computing facility. Future work should focus more on the multiphase modelling aspects. Whilst opportunities exist for particle tracking using a Lagrangian model, few workers have attempted this. The fractal nature of flocs poses limitations on the accuracy of the results generated and, in particular, the impacts of density and porosity on drag force and settlement characteristics require additional work. There is significant scope for the use of coupled population balance models and CFD to develop water treatment flocculation models. Results from related work in the wastewater flocculation field are encouraging.

Keywords: computational fluid dynamics, turbulence, flocculation, mixing, multiphase modelling, fractal dimension

1. INTRODUCTION

The scope for applying CFD to flow problems in the water industry is large, with raw water reservoirs, water treatment works, distribution systems (including treated water storage), collection systems, and sewage treatment works all involving large scale fluid flow. Using CFD it is possible to derive the information necessary to design, optimise or retrofit various treatment processes. Further advantages include reduced lead-in times and costs for new designs, the ability to examine the behaviour of systems at the limit or beyond design capacity, and the ability to study large systems where controlled experiments at full-scale would be difficult, if not impossible, to perform.

Effective water treatment to potable standards involves a complex system of physical, chemical and biological processes, all occurring in a wide range of hydrodynamic environments. Whilst much research effort has been devoted to chemical process optimisation, there remains the need to understand fully the inter-relationships

between chemical and biological reactions and the hydraulic conditions within which they occur. An insight into the relationships between hydrodynamics and water chemistry in particular can facilitate the optimisation of existing plant and machinery and the development of novel design criteria for new unit processes. Such new, optimised design criteria enable water utilities to derive greater efficiencies by reducing capital expenditure on new assets, reducing operational expenditure on existing assets, and also reducing chemical and energy input.

The use of CFD, whilst traditionally strong and widespread in the chemical, mechanical and manufacturing industries, has only begun to be exploited within the water industry relatively recently. However, interest and experience in this field are both growing apace, and CFD has now been successfully used in water and sewage treatment and sewerage applications, both in the UK and abroad. Examples of water treatment applications are now many and varied. However, whilst CFD has proven to be of use in understanding the standard hydrodynamics of

flow processes in structures, there remain certain areas which involve greater degrees of computational complexity and where further improvements are still required. One such example is flocculation.

2. FLOW REGIMES AND SCENARIOS FOUND IN WATER TREATMENT

2.1 Background

Water treatment is based on a series of unit processes, each effecting some degree of removal or inactivation of impurities, ranging in size from millimetres (grit, leaves) to microns (colloids, viruses, protozoa). The principal processes involved in water treatment are identified in Table 1. Successful removal of these impurities requires a range of different flow regimes throughout a water treatment works (WTW). The accurate modelling of each process and flow regime requires careful consideration, as each presents its own subtleties and issues. Examples of the range of flow regimes and possible CFD modelling approaches are given in Table 2.

Table 1 Overview of principal water treatment processes.

Treatment Process	Description	Purpose
Raw Water Storage	Bulk storage of water > 1 day.	Backup supply to WTW in event of source pollution. Some solids removal via sedimentation.
Coagulation	Chemical (trivalent inorganic coagulant) dose and short (<30 s) rapid mix.	Destabilisation of water via neutralization of colloidal material charge and precipitation of soluble compounds.
Flocculation	Slow, extended (15–45 mins) mix.	Encourage agglomeration of particles to form mass fractal aggregates ("flocs") up to 1000 μm.
Clarification	Sedimentation or flotation (via dissolved air injection) of larger flocs.	Solids removal.
Filtration	Flow through porous granular media.	Removal of smaller flocs and particles (<100 μm).
Disinfection	Chemical (chlorine, UV) dose and storage (chlorine only).	Killing or inactivation of potentially harmfully micro-organisms.

Table 2 Flow regimes and CFD modelling approaches adopted in water treatment.

Flow Characteristics	Treatment Process	CFD Modelling Approach
Turbulent flow	• Open channel flow • Pipe flow • Mixing chambers	• 2-equation turbulence models • Reynolds Stress Model • Large Eddy Simulation • Direct Numerical Simulation
Laminar flow	• Settlement tanks	• Laminar flow model
Multiphase flow	• Coagulation • Flocculation • Settlement • Flotation • Filtration • Disinfection	• Eulerian multiphase model • Lagrangian particle model
Rotating flow	• Mixing chambers • Flocculation	• Sliding Mesh • Multiple Reference Frames

2.2 Turbulence modelling

Most water treatment processes take place in turbulent flow regimes. The most straightforward complete turbulence models are the two-equation models where the turbulent velocity and length scales are determined via solution of two separate transport equations; one for turbulent kinetic energy, k, and one for the turbulence length scale or some equivalent parameter (ε, the dissipation of turbulence kinetic energy per unit time, or ω, the rate at which turbulent energy is dissipated). These equations account for the production, diffusion and destruction of turbulence within the flow field. The principal assumptions for these models are that the flow does not depart far from local equilibrium, and that the Reynolds number is high enough to ensure that local isotropy is satisfied.

Two-equation turbulence models are based on the eddy viscosity concept of Boussinesq. This eddy-viscosity model states that the Reynolds stresses are related to the local shear via eddy viscosity, v_t, in the following manner (Rodi, 1993):

$$-\overline{u_i u_j} = v_t \left(\frac{\partial U_i}{\partial x_j} + \frac{\partial U_j}{\partial x_i} \right) - \frac{2}{3} k \delta_{ij} = 2v_t s_{ij} - \frac{2}{3} k \delta_{ij}$$

$$(1)$$

The turbulent eddy viscosity, v_t, is defined in terms of the turbulent kinetic energy, k, and the rate of dissipation of turbulent energy per unit mass, ε, according to:

k-ε model:
$$v_t = C_\mu \frac{k^2}{\varepsilon} \qquad (2)$$

k-ω model:
$$v_t = C_\mu \frac{k}{\omega} \qquad (3)$$

$$k = \frac{u_i u_j}{2} \text{ and } \varepsilon = v \frac{\partial U_i}{\partial x_j} \left(\frac{\partial U_i}{\partial x_j} + \frac{\partial U_j}{\partial x_i} \right) \qquad (4)$$

δ_{ij} represents the Kronecker delta and is defined as:

$$\delta_{ij} = \begin{cases} 1 & i = j \\ 0 & i \neq j \end{cases} \qquad (5)$$

A detailed discussion of the terms in the k-ε models can be found in Launder and Spalding (1974). The principal turbulence models which are generally packaged with commercially available CFD packages are the standard k-ε model, the low Reynolds number k-ε model (LRN k-ε), the renormalized group k-ε model (RNG k-ε), the realizable k-ε model, the standard k-ω model, the shear-stress transport (SST) k-ω model, and

the Reynolds stress model (RSM). In addition, most codes provide the Spalart-Allmaras model, and the Large Eddy Simulation (LES) model. A descriptive comparison of the most commonly used turbulence models is provided in Table 3 and the formulation of each is presented in Appendix 1.

3. FLOCCULATION MODELLING

3.1 Background

The destabilisation (via coagulation) and subsequent agglomeration (via flocculation) of fine particles and colloids into larger particles is a proven means of removing impurities (e.g. turbidity and colour) at WTWs. Chemical coagulant addition brings about a change in the nature of small particles, reducing their negative surface charge and rendering them unstable, whilst flocculation encourages particle agglomeration via gentle mixing and the formation of irregularly-shaped, loosely connected mass fractal aggregates, known as flocs. The size and structure of flocs are fundamental to the efficient operation of WTWs. Ineffective coagulation and flocculation result in poorer quality feed water to downstream treatment processes, potentially jeopardising treated water quality and increasing operational costs. Several interrelated criteria govern the efficiency of the coagulation and flocculation stages; viz. coagulant type and dosage, pH and mixing arrangements.

Flocculation is the transformation of smaller destabilised particles into larger aggregates or flocs which are subsequently removed via sedimentation or flotation processes. For all flocs in their initial growth phase, the floc formation process is understood to be a balance between the rate of collision-induced aggregation and the rate of breakage for given shear conditions (Bouyer et al., 2005; Mikkelsen, 2001; Biggs and Lant, 2000).

$$R_{floc} = \alpha_{ij} R_{col_{ij}} - R_{br} \qquad (6)$$

where R_{floc} is the overall rate of floc growth, α is the collision efficiency factor ($0 < \alpha < 1$), R_{col} is the rate of particle collision and R_{br} represents the rate of floc breakage.

Table 3 Comparison of available turbulence models (from Versteeg and Malalasekera, 1995, Marshall and Bakker, 2004, and Menter, 2003).

Model	Comments	Advantages	Disadvantages
Standard k-ε	• Semi-empirical modelling of *k* and *ε*. • Valid for full turbulence only (molecular diffusion ignored).	• Simplest model. • Excellent performance for many flows. • Well established.	• Poor performance in some scenarios (i.e. rotating flows, flow separation, adverse pressure gradients). • Assumes isotropy in turbulence. • Poor prediction of lateral expansion in 3-d wall jets.
Renormalized Group (RNG) k-ε	• Based on statistical methods, not observed fluid behaviour. • Mathematics is highly abstruse. Texts only quote model equations which result from it. • Effects of small-scale turbulence represented by means of a random forcing function in N-S equations. • Procedure systematically removes small scales of motion by expressing their effects in terms of larger scale motions and a modified viscosity. • Similar in form to *sk-ε*, but modified dissipation equation to describe high-strain flows better. • Differential equation solved for μ_t (changes C_μ from 0.09 to 0.0845 at high Re), so good for transitional flows.	• Improved performance for swirling flow compared to the standard *k-ε* model.	• Less stable than the standard *k-ε* model.

Table 3 (Continued)

Model	Comments	Advantages	Disadvantages
Realizable k-ε	• Recent development. In highly strained flows, the normal Re stresses, u_i^2, become negative (unrealizable condition), so μ_t uses variable C_μ. • C_μ is function of local strain rate and fluid rotation. • Different source and sink terms in transport equations for eddy dissipation. • Good for spreading rate of round jets.	• Suited to round jets, as well as swirling flows and flows where separation occurs.	• Not recommended for use with multiple reference frames.
Standard k-ω	• $\omega = \varepsilon/k$ = specific dissipation rate. • s*k-ε* solves for dissipation of turbulent kinetic energy, *k-ω* solves for rate at which dissipation occurs. • Resolves near wall without wall functions, so can be applied through boundary layer.	• Valid throughout the boundary layer, subject to sufficiently fine grid resolution.	• Separation is typically predicted to be excessive and early.
Shear Stress Transport (SST) k-ω	• As *k-ω* except for gradual change from *k-ω* in inner region of boundary layer to high Re version of s*k-ε* in outer part. • Modified μ_t formulation to account for transport effects of principal turbulent shear stresses.	• Suitable for adverse pressure gradients and pressure-induced separation. • Accounts for the transport of the principal turbulent shear stress.	• Less suitable for free shear flows.
Reynolds Stress Model	• The most general of all models.	• Accurate calculation of mean flow properties and all Reynolds stresses. • Yields superior results to *k-ε* models for flows with stagnation points.	• Computationally expensive. • Not always more accurate than two-equation models. • Harder to obtain converged result.

More accurately, the $\alpha_{ij} R_{col_{ij}}$ term should be broken down further into its constituent parts where $\alpha_{ij} R_{col_{ij}}$ is a function of

$$^{BM}\alpha_{ij}\,^{BM}R_{col_{ij}},\ ^{Sh}\alpha_{ij}\,^{Sh}R_{col_{ij}},\ \text{and}\,^{DS}\alpha_{ij}\,^{DS}R_{col_{ij}} \qquad (7)$$

where i and j refer to discrete particles, and *BM*, *Sh* and *DS* refer to the collision mechanisms of Brownian Motion, shear and differential settlement respectively. (Derivations of these mechanisms are to be found in the literature, e.g. Kusters, Wijers and Thoenes, 1997). As a result, flocs do not continue to grow throughout the flocculation stage, but rather, they attain a limiting size beyond which breakage prevents further overall growth. The flocculation process, and hence this limiting size, is governed by physico-chemical conditions and by the shear conditions within the containing vessel. Bouyer et al. (2005) investigated the link between hydrodynamics, physico-chemical conditions and floc size, and found a dependency of floc size on hydrodynamic history. Consequently, vessel hydrodynamics exhibit significant control over the effectiveness of flocculation.

Particle removal efficiency decreases with decreasing particle size (Boller and Blaser, 1998). Therefore, flocs must be able to withstand shear energy applied to them in various different unit processes; otherwise, when the degree of shear exceeds a threshold value, floc breakage will occur. However, quantification of the energy requirements for floc breakage is not straightforward, and despite much work in this field, no standard strength test exists. Thus, effective and efficient modelling of the various types and configurations of flocculators presents some excellent opportunities, but also some specific and interesting challenges for the modeller.

Flocculation at WTWs is effected either via mechanical or hydraulic means. For mechanical flocculation, the energy input is via an agitator which generates the necessary shear stress, whereas in hydraulic flocculation, energy is imparted via the headloss across a baffled, serpentine channel. The two processes are shown schematically at Fig. 1.

Coagulation and flocculation optimisation are generally considered at the laboratory scale, using a jar test apparatus and procedure. This well-established process optimisation technique allows a rapid assessment of key variables (e.g. coagulant dose, pH, mixing speed and flocculation time). The test apparatus typically comprises four or six glass vessels, each with a powered paddle to stir the contents of the vessel and each containing the same volume of raw water. The paddles are set to rotate at high speed for a short period, during which time different quantities of coagulant (and acid or alkali for pH adjustment as necessary) are added to each vessel and mixed. After a short period of intense mixing (30–60 seconds) to simulate the coagulation process, the paddle speed is reduced to produce a more gentle mixing to simulate the flocculation process. After 20 minutes of flocculation, mixing is terminated, the paddles removed and the suspensions allowed to settle. The flocs and treated water in each vessel are then analysed for floc size, turbidity removal and organics removal, allowing conclusions to be drawn regarding optimum coagulant dose and pH. These conclusions are often then applied to the operation of the main treatment plant. Two typical jar test configurations are shown at Fig. 2.
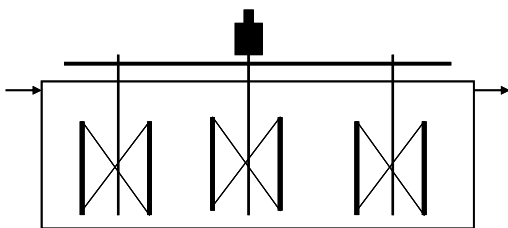

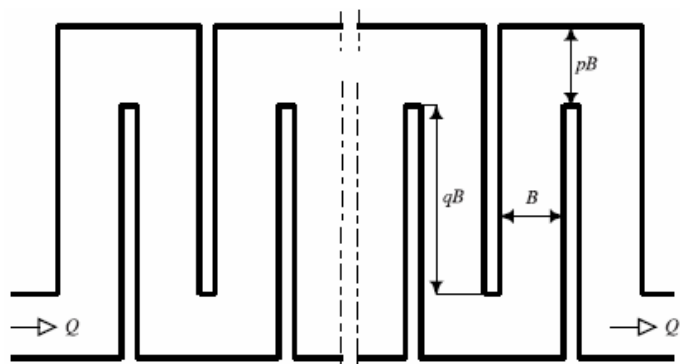Fig. 1a   Schematic diagram of sectional view of a mechanical flocculator.

Fig. 1b   Schematic diagram of plan view of an hydraulic flocculator, from Haarhoff and Van der Walt (2001).
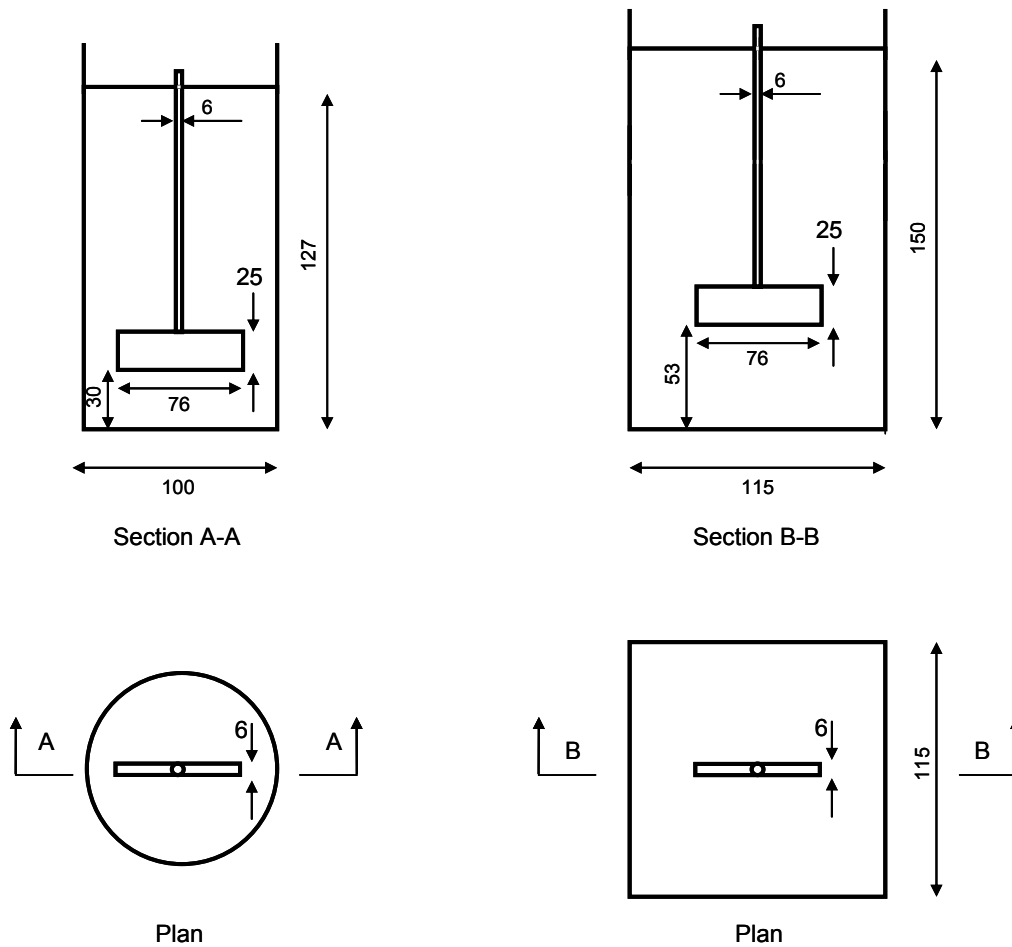
Section A-A

Plan

Section B-B

Plan

Fig. 2   Typical jar test vessel configurations (not to scale, all dimensions in millimetres).
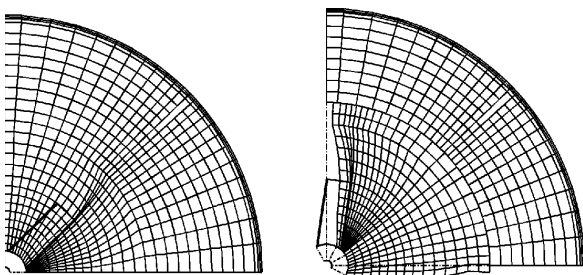

Fig. 3   Sliding mesh in two orientations, shown in 2D, from Marshall and Bakker (2004).

3.2   Rotating flow

The modelling of rotating flows (such as those found in mechanical flocculation) is of great importance in mechanical flocculation and a number of approaches are available to the modeller to represent this scenario. The traditional approach to modelling paddle mixers was to apply experimentally-obtained velocity data in the outflow of the impeller. However, such methods have now largely been superseded

by explicit calculation of the flow pattern in the vicinity of the blades without recourse to experimental data. This is to be favoured above the application of experimental data, since it avoids the need to extrapolate any such experimental data in order to apply it to situations for which no experiments have been, or can be, performed.

One method of explicitly calculating the flow field in a rotating flow scenario is the sliding mesh method. With the sliding mesh method, the tank is divided into two regions that are treated separately: 1) the impeller region and 2) the tank region which includes the bulk of the liquid, the tank wall, the tank bottom and the baffles (Fig. 3). The grid in the impeller region rotates with the impeller, whilst the grid in the tank remains stationary. The two grids slide past each other at a cylindrical interface. The sliding grid model explicitly calculates the mixer region, and then rotates this section of the grid relative to the rest of the domain. It is assumed that the flow field is unsteady, and the interactions are modelled as

they occur. Consequently, the sliding mesh model is the preferred option in instances where interaction between rotor and baffle is strong and the most accurate simulation of the system is desired. Whilst the sliding mesh model is the most accurate method for simulating flows in multiple moving reference frames, it is also the most computationally demanding. Using the sliding mesh model to analyse laminar flows in a stirred reactor, Bakker et al. (2000) used a time step of 0.01 s and 1000 time steps to study the flow created by a pitched blade turbine in a tank. With an impeller rotational speed of 3.75 s^{-1}, 37.5 revolutions were simulated. Bakker et al. reported that the calculation time was approximately 15 minutes per impeller revolution on a Cray C-90 computer, giving a total CPU usage time of 9.75 hours.

An alternative means of modelling the mixing process is to use the Multiple Reference Frames (MRF) approach (Luo, Issa and Gosman, 1994). This approach adopts two reference frames; one stationary frame related to the vessel walls; the other related to the rotating shaft and impeller. The fluid zone is divided into two separate regions, one of which is related to the stationary zone, whilst the other, close to the rotating impeller, is related to the moving zone (Fig. 4). The momentum equations and closure models are resolved in the separate zones and a steady-state approximation is made at the zone interface. The mesh does not move in this technique. The MRF is computationally far more expedient than the sliding mesh method and for steady state applications has been used successfully to model mixing systems of various types. However, if an unsteady solution is required, the sliding mesh approach is the method of choice.
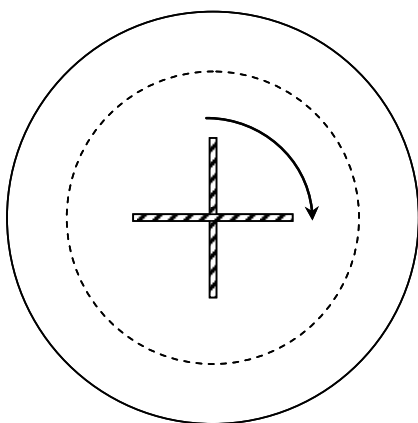

Fig. 4 Cylindrical mixing tank with an MRF boundary surrounding the impeller, from Fluent (2005).

3.3 Swirling flow

The mechanical mixing of flocculators can often result in swirling flow conditions, thus introducing anisotropic turbulence conditions, and so presenting some specific and interesting challenges. Although two-equation models are commonly used by CFD practitioners, these models exhibit an inherent difficulty when modelling swirling flow as they are predicated on the assumption that turbulence is isotropic, meaning that the turbulent stress tensor is independent of direction (or, more precisely, invariant with respect to rotation and reflection of the coordinate axes of the coordinate system moving with the mean motion of the fluid). This assumption is not true for swirling flow which is anisotropic in nature and where turbulence is generally more in the tangential and axial directions compared to the radial direction. Therefore, in order to capture this anisotropic nature of turbulence, other models (e.g. RSM) should be employed as the effects of strong turbulence anisotropy can be modelled rigorously only by the second-moment closure adopted therein. It is widely acknowledged that the RSM is the most rigorous of the available models (Versteeg and Malalasekera, 1995); however, this additional rigour comes with concomitant additional computational power and time.

Irrespective of the above comments, it is interesting to note that the literature contains several examples of the use of two-equation models to solve highly swirling flow conditions (e.g. Ducoste and Clark, 1999; Korpijarvi et al., 1999; Korpijarvi, Laine and Ahlstedt, 2000; Essemiani and de Traversay, 2002a & b; Ng, Borrett and Yianneskis, 1999). Korpijarvi et al. (1999) modelled the flow patterns found within a cylindrical jar test device. Grids of 30,000 and 67,000 cells were developed to represent the vessel and the authors tested the sensitivity of the flow patterns within the two grids to four different turbulence models; viz. standard k-ε, RNG k-ε, LRN k-ε and the RSM, used in conjunction with the Sliding Mesh approach. Velocities within the mini-flocculator were found to be insensitive to changes in turbulence model or grid density. Korpijarvi et al. demonstrated that the total dissipated power in the fine grid mesh was more than twice that found in the coarser mesh. The difference observed by the authors when comparing total dissipated power associated with LRN k-ε and RSM models using the coarse grid rose to in excess of ten-fold,

demonstrating the importance of turbulence model selection.

All turbulence models offer advantages and disadvantages over others in certain applications, and no single turbulence model can be judged to be the optimum model in all circumstances. Consequently, it is necessary to evaluate each circumstance individually and form a view as to which model would provide the best fit for the particular flow under examination. Factors to consider include, inter alia, the physics encompassed in the flow, the established practice for a specific class of problem, the level of accuracy required, the available computational resources, and the amount of time available for the simulation. It is clear from the above that the selection of turbulence model is not a straightforward one. Menter (2003) correctly suggested that one should resist the temptation to claim that one model is superior to another, as the robustness of a turbulence model is undoubtedly a function of the code being used and the scenario being modelled. This has been reaffirmed by several authors (e.g. Freitas, 1995; Iccarino, 2000) who urged caution in the unilateral promotion of one code, turbulence model, convergence criteria or discretisation technique at the expense of all others. Specific factors relating to the scenario being analysed must always be accounted for.

The situation is further complicated by the fact that in a jar tester, the highly swirling, anisotropic nature of the flow often leads to the formation of a surface vortex. Using CFD it is possible to track the shape of the liquid surface during mixing using the Volume of Fluid (VOF) Model. In this approach, the computational domain is extended beyond the surface to span the air/water interface, and the volume fraction of each phase is determined throughout the flow field by solving the continuity equation for one of the phases. Although most often applied to an air/water interface in water treatment applications, the VOF model can be applied to any number of immiscible fluids, subject to computational power. For an homogeneous multiphase system consisting of air and water, the equation is solved for the volume fraction of the liquid phase. In a given computational cell, the volume fraction of unity represents pure water and zero represents pure air. Thus, the volume fraction of the air is obtained as the difference between the liquid phase volume fraction and unity. The air/water interface is determined by identifying the cells where the volume fraction is between zero and unity. Thus,

if the volume fraction of water in any given cell is represented by α_w, then,

$\alpha_w = 0$ implies that the cell is empty of water, $\alpha_w = 1$ implies that the cell is full of water, and $0 < \alpha_w < 1$ implies that the cell contains the air/water interface.

Haque, Mahmud and Roberts (2006) simulated the flow field in unbaffled vessels mixed with a paddle impeller and a Rushton turbine and adopted the VOF approach to represent the vortex formed at the surface. Using the MRF approach to rotating flow and the RSM to model turbulence, Haque, Mahmud and Roberts (2006) reported a typical run time of 70 hours to achieve convergence (Sun UltraSPARC III processor, 4Gb RAM, 900 MHz clock speed). Thus, it can be seen that the computational expense of considering the liquid surface shape is significant. Whilst the authors reported reasonable correlation between observed and numerically-obtained vortex shapes, they found discrepancies between the predicted and measured values in the vicinity of the shaft. Haque, Mahmud and Roberts (2006) also compared axial velocities at various locations, but did not consider turbulence quantities. Despite the reasonable results obtained by Haque, Mahmud and Roberts, it is noteworthy that Marshall and Bakker (2004) recommended that this approach should not be adopted for the prediction of vortex shape. Marshall and Bakker recognized that the VOF model has application in the monitoring of liquid surface shape, but suggested that the model is ill-equipped to deal with the bubble formation arising from the breaking of the air/water interface when air passes through grid cells where large momentum sources exist. As a result, Marshall and Bakker (2004) concluded that it is appropriate to use the VOF model to indicate whether or not vortexing will occur, but that it should not be used to predict the flow condition afterwards.

3.4 Velocity gradient

Traditionally, flocculators have been characterised on the basis of the velocity gradient (Camp and Stein, 1943). This parameter is used worldwide to characterize mixing in a wide range of environmental engineering applications, and principally mixing in flocculation basins (e.g. Crittenden et al., 2005). From the consideration of the angular distortion of an elemental volume of water arising from the application of tangential surface forces, G is defined as the root mean square velocity gradient in a mixing vessel:

$$G = \left\{ \left(\frac{\partial u}{\partial y} + \frac{\partial v}{\partial x} \right)^2 + \left(\frac{\partial u}{\partial z} + \frac{\partial w}{\partial x} \right)^2 + \left(\frac{\partial v}{\partial z} + \frac{\partial w}{\partial y} \right)^2 \right\}^{0.5} \quad (8)$$

where u, v and w are the velocity components in the x, y and z directions of a Cartesian coordinate system.

Camp and Stein termed this the absolute velocity gradient and related this to work done per unit volume per unit time via:

$$\Phi = \mu\, G^2 \quad (9)$$

From which:

$$G = \sqrt{\frac{P/V}{\mu}} = \sqrt{\frac{\varepsilon}{v}} \quad (10)$$

where
- Φ work of shear per unit volume per unit time at a point
- P is power dissipated
- V is tank volume
- μ is the dynamic viscosity of the water,
- ε is the energy dissipation rate per unit mass
- v is the kinematic viscosity of the water

In theory, the absolute velocity gradient can be calculated at any point within a mixing vessel, provided that the power dissipated is known at that point. In practice, however, the flow characteristics vary within the mixing vessel from point to point, and so too does the energy dissipation. Consequently the velocity gradient is a function of both time and position. Given the difficulties associated with calculation of G, workers have traditionally replaced the absolute velocity gradient with an approximation of the exact value; that is its average value throughout the vessel, $\overline{G}$:

$$\overline{G} = \sqrt{\frac{P_{ave}}{V\mu}} \quad (11)$$

where the average power consumption, P_{ave}, is readily obtained via

$$P_{ave} = P_o\, \rho\, N^3\, D^5 \quad (12)$$

where
- P_o is the impeller power number
- ρ is the fluid density
- N is the rotational speed of the impeller
- D is the impeller diameter

Since its introduction, authors have argued that the concept of the $\overline{G}$ value is flawed, as it attempts to represent a complex flow field within a single number (Cleasby, 1984; Clark, 1985; Graber, 1994; Luo, 1997; Jones, 1999). Furthermore, the distribution of velocity gradients within a stirred tank is clearly not uniform, and local power consumption at a point of high turbulence within a vessel (e.g. adjacent to the impeller) can be several orders of magnitude in excess of the rest of the vessel (Luo, 1997). When considering flocculation, this is unfortunate as it is precisely the magnitude and fluctuations in local shear to which a floc is subjected, and not the average value, which determine the success of flocculation.

However, using CFD it is possible to quantify and understand the local impact of mean flow and turbulence on floc formation and break-up using the local velocity gradient, G_L, where

$$G_L = \sqrt{\frac{\varepsilon}{v}} \quad (13)$$

Korpijarvi, Laine and Ahlstedt (2000) demonstrated the very large variability of the local velocity gradient value (G_L) within a jar test vessel, thus questioning the validity of the use of the $\overline{G}$ value to characterise the vessel. Unsurprisingly, the largest G_L values were to be found near the paddles and particularly in the turbulent area behind the panel, stretching in a radial direction towards the wall.
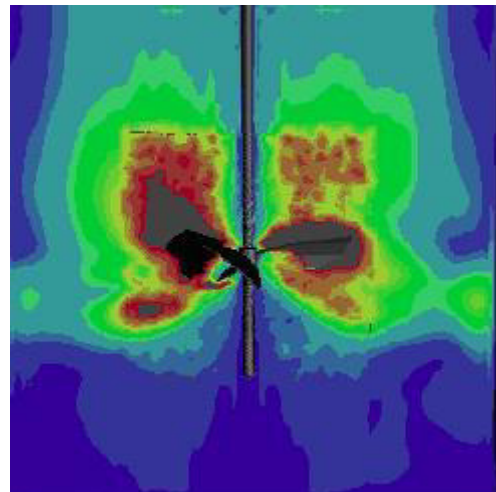

Fig. 5   Distribution of local velocity gradients in a pilot scale mechanical flocculator. Flow rate = 2 m³.hr⁻¹, mixing speed = 73 rpm, from Essemiani and de Traversay (2002a).

Essemiani and de Traversay (2002a) modelled a pilot scale mechanical flocculator to determine areas of highest shear stress (where floc break-up is to be anticipated) and also areas of the lowest

values where, subject to a de minimus, one would expect coalescence (i.e. floc growth) to occur. Similar to Korpijarvi et al. (1999) and Korpijarvi, Laine and Ahlstedt (2000), the authors found that the distribution of local velocity gradients indicated high G_L intensity adjacent to the impeller, decreasing with distance from it (Fig. 5).

Essemiani and de Traversay (2002a) found that for the system considered, $\overline{G}$ and the average G_L values exhibited reasonably close correlation, although there was a great range of G_L values; a conclusion corroborated by Bridgeman, Jefferson and Parsons (2008). Essemiani and de Traversay concluded that $\overline{G}$ does not account for variables such as impeller position, geometry, operating mode and residence time. However, these parameters do affect the velocity gradient distribution, and therefore, spatial floc size distribution. As a result, Essemiani and de Traversay suggested that for the same $\overline{G}$ value, changing mixing rates and impeller type will affect performance.

Craig et al. (2002) developed a model using Fluent to simulate the operation and performance of a simple flocculation tank equipped with an axial impeller generating turbulent flow conditions. No details of modelling technique or turbulence model used were provided. Craig et al. used the model to demonstrate variations in the G_L value, and to identify maximum and minimum G_L values associated with different operational scenarios. The authors identified that use of G_L values in this manner enabled the identification within the flocculation tank of those areas where both coalescence and floc break-up would occur. Similar to Essemiani and de Traversay (2002a), this led the authors to question the validity of the use of the $\overline{G}$ value as a design parameter.

Haarhoff and van der Walt (2001) used the lesser-used Flo++ code to study flow in an around-the-end hydraulic flocculator. Building on previous work (van der Walt, 1998), Haarhoff and van der Walt used CFD to develop qualitative guidelines for three fundamental geometric ratios (slot width ratio, overlap ratio and depth ratio) (see Fig. 1b). No details of modelling strategy were provided in the paper.

Haarhoff and van der Walt also studied the variation of the $\overline{G}$ value in hydraulic flocculators. It is known that hydraulic flocculators incur zones of high turbulence at the baffle edges which can cause floc break-up. The authors showed variations in G_L in the flocculator in both

absolute terms and normalized by dividing by the $\overline{G}$ value. They then introduced the concept of a 95th percentile of the normalized G value distribution in the flocculator as an arbitrary (but, in their opinion, realistic) performance indicator for flocculator optimisation (i.e. a G value which is exceeded only in 5% of the total flocculator volume). The authors argued that use of this G_{95} figure enables the designer to compare absolute and normalized G values on a more representative basis than by simply using the average. Using this approach, Haarhoff and van der Walt were able to conclude that the slot width ratio is the single most important geometric ratio for design purposes. The effect of the overlap ratio was found to have a less pronounced impact on the G values, whilst the effect of the depth ratio was inconsequential if the channel velocity was maintained.

3.5 Floc breakage

Having expended time and energy in developing flocs, it is important that operating conditions do not subsequently cause their break-up. As a result, floc strength, growth and breakage have been the subject of detailed research in recent years.

Floc size may be considered to be a balance between the hydrodynamic forces exerted on a floc and the strength of the floc. Where the floc strength is resistant to the hydrodynamic forces, one would expect floc size either to remain constant or for growth to occur. Where the hydrodynamic forces exceed floc strength, breakage will occur. Consequently, the conceptual growth/breakage mechanism may be expressed as follows:

$$B = \frac{\text{Hydrodynamic Forces}}{\text{Floc Strength}} = \frac{F}{J} \qquad (14)$$

where F represents the hydrodynamic forces exerted by the flow, and J represents the strength of the floc (Coufort, Bouyer and Liné, 2005). It is clear from Eq. (14) that breakage will occur when $B > 1$, and floc size will be maintained or increased when $B < 1$. Floc strength, J, is a function of the physico-chemical conditions (raw water type, coagulant type and dose) and the floc structure.

Yeung, Gibbs and Pelton (1997) suggested that the hydrodynamic force required to pull apart a floc in tensile mode may be expressed as:

$$F \approx \frac{\pi}{4}.\sigma.d^2 \qquad (15)$$

where F represents the floc rupture force, σ represents the floc strength, and d is the floc diameter. In the viscous sub-range, $\sigma = \mu.\sqrt{\varepsilon/\nu}$. Substituting into Eq. (14) shows that the breakage mechanism in the viscous sub-range, B_{VSR}, may be expressed as:

$$B_{VSR} = \frac{C_1 \mu \sqrt{\varepsilon/\nu}.d^2}{J} \qquad (16)$$

where C_1 is a constant.

Thomas (1964) suggested that in the inertial sub-range

$$\sigma = \overline{\rho.u}'^2 \text{ and } \overline{u}'^2 = C_2(\varepsilon.d)^{\frac{2}{3}} \qquad (17) \& (18)$$

Substituting into Eq. (14) shows that the breakage mechanism in the inertial sub-range, B_{ISR}, may be expressed as:

$$B_{ISR} = \frac{C_2 \rho \varepsilon^{\frac{2}{3}}.d^{\frac{8}{3}}}{J} \qquad (19)$$

where C_2 is a constant.

Consequently, it is apparent from Eqs. (16) and (19) that floc size is dependent on the turbulence energy dissipation rate and floc strength, irrespective of sub-range. This is clearly of great significance when one attempts to gain an understanding of floc breakage mechanisms and limiting floc size as it directs workers to focus their towards ε and J.

Essemiani and de Traversay (2002a & b) argued that the G_L distribution (and, hence, ε distribution) in a vessel is significant as it controls particle suspension, distribution, coalescence and break-up efficiency. The authors did not, however, attempt to quantify the effects of local shear on floc characteristics; a subject addressed by Bridgeman, Jefferson and Parsons (2008) who used CFD coupled with a Lagrangian particle trajectory model to model the flow field within a standard jar test apparatus to study the effects of turbulence on individual flocs. Combining numerical and experimental data, the authors were able to postulate velocity gradient values at which floc breakage occurs for three different floc suspensions. Although the threshold values were determined using jar test and CFD data in combination, they were based on the flocs' resistance to induced velocity gradients. This is a significant result, as previous breakage thresholds had always been expressed in terms of mixing speed and so could not be applied at full scale. The results of Bridgeman, Jefferson and Parsons (2008) can be adopted for use in other situations and can be used to assess the

performance of existing flocculators or to design new installations, thus permitting optimisation on the basis of implied floc strength. Indeed, Bridgeman, Jefferson and Parsons (2007) modelled two full scale flocculators (one mechanically mixed, the other an hydraulic installation) and assessed their performance in terms of the breakage threshold concept. However, the computational expense of using sliding mesh to model a three dimensional full scale flocculator using the realizable k-ε model was significant. (Using a high performance computing facility, the full scale mechanical flocculator sliding mesh simulations required up to 12 days' CPU usage).

3.6 Residence time distribution

One means by which flocculator performance can be assessed is by considering the residence time of flocs. Empirical guidelines exist regarding optimum residence times for flocs, and CFD can be used to gain an improved understanding of retention times in vessels.

Although it is possible to employ the discrete phase model to undertake a Lagrangian particle tracking analysis on a number of particles to determine overall residence times, this method requires a large number of particles to be analysed in order for the results to be statistically valid and so introduces significant additional computational expense and time. An alternative approach is to treat a tracer fluid as a continuum by solving a transport equation for the tracer species. The transport and decay of a chemical species in a flow can be described by a general convection/diffusion equation:

$$\rho \frac{\partial \phi}{\partial t} + \rho u_i \frac{\partial \phi}{\partial x_i} - \left(\rho D_\phi + \frac{\mu_t}{\sigma_\phi} \right) \frac{\partial^2 \phi}{\partial x_i^2} = S \qquad (20)$$

where ϕ is any scalar variable, D_ϕ is the molecular diffusivity of the scalar, σ_ϕ is the turbulent Schmidt number of the scalar, and S is the source/sink term for the scalar variable ($= 0$ for tracer transport).

The residence time distribution (RTD), $E(t)$ is a measure of the bulk flow patterns in a vessel and is defined such that the RTD function represents the fraction of fluid at the outlet that has a residence time in the vessel of between t and $t + \delta t$. Consequently,

$$\int_0^\infty E(t)dt = 1 \text{ and } \int_{t_1}^\infty E(t)dt = 1 - \int_0^{t_1} E(t)dt \qquad (21)$$

To assess RTD numerically, a small amount of non-reactive tracer (approximately 0.5% of vessel volume), with fluid properties set to the same as water, is "injected" into the flow via the inlet. All reactions between the species and bulk flow are turned off, and the species concentration monitored at the outlet. It is normal for the tracer study data to be normalised on the basis of $\bar{t}$ and C_N where

$$\bar{t} = \frac{\int_0^\infty Ct\,dt}{\int_0^\infty C\,dt} \approx \frac{\sum \overline{Ct}\,\Delta t}{\sum \overline{C}\,\Delta t} \qquad (22)$$

$$C_N = \int_0^\infty Cd\left(\frac{t}{\bar{t}}\right) = \frac{\int_0^\infty Cdt}{\bar{t}} \approx \frac{\sum \overline{C}\Delta t}{\bar{t}} \qquad (23)$$

$$E(\theta) = \frac{C}{C_N} \qquad (24)$$

where $\bar{t}$ = mean residence time in vessel,

C = concentration exiting vessel at time t,

t = time since addition of tracer pulse to vessel.

Crittenden et al. (2005) presented the key terms used to characterise RTD curves and these are presented in Table 4.

3.7 Multiphase modelling

3.7.1 Background

Much of the CFD modelling of flocculators has considered the bulk flow characteristics of specific vessels. Examples of CFD flocculation modelling are to be found in Table 5. It is possible, however, to use CFD to consider floc transport analysis in flocculators. Using a Lagrangian approach, the predicted pathlines of particles, varying in both size and density, can be studied.

3.7.2 Lagrangian particle model

Treating each particle individually, the Lagrangian particle model solves the equations of motion for each particle to obtain its trajectory in space and time. Equations for temperature and species concentration can be added to model heat and mass transfers between the particles and the surrounding fluid, thus yielding detailed information regarding the particles, their positions (in both space and time), trajectories, temperature and species concentration.

Table 4 RTD curve characterisation terms, from Crittenden et al. (2005).

Term	Definition
t	Theoretical hydraulic retention time, $= V/Q$
t_i	Time at which tracer first appears
θ	Normalised retention time $= t/\bar{t}$
t_p	Time at which peak concentration of tracer is observed
$\bar{t}$	Mean residence time $=$ centroid of $E(\theta)$ curve
t_{10}, t_{50}, t_{90}	Time at which 10, 50 and 90% of tracer has passed through reactor
t_{50}/t_{90}	Morrill dispersion index
t_i/τ	Index of short-circuiting. Ideal plug flow reactor $= 1$. Tends to 0 with increased short-circuiting
t_{50}/τ	Index of mean retention time. Measure of skew of $E(\theta)$ curve

Table 5 CFD modelling of flocculation processes.

Author	Code	Aim	Scale	Dim	Turb. Model	Extra Model	Validation method
Ducoste & Clark, 1999	FIDAP	Code evaluation for modelling flocculator fluid mechanics.	Lab	3D	$sk\text{-}\varepsilon$	None	LDV
Bridgeman, Jefferson & Parsons, 2008	Fluent	Evaluation of floc strength and trajectory in jar tester.	Lab	3D	$sk\text{-}\varepsilon$, $Rz\ k\text{-}\varepsilon$, $RNG\ k\text{-}\varepsilon$, $k\text{-}\omega$, $SST\ k\text{-}\omega$, RSM	DPM	LDA
Bridgeman, Jefferson & Parsons, 2007	Fluent	Flow characteristics in two jar test configurations.	Lab	3D	$sk\text{-}\varepsilon$, $Rz\ k\text{-}\varepsilon$, $RNG\ k\text{-}\varepsilon$, $k\text{-}\omega$, $SST\ k\text{-}\omega$, RSM	DPM	LDA, PIV
		Flow characteristics in mechanical flocculator.	Full		$sk\text{-}\varepsilon$, $Rz\ k\text{-}\varepsilon$, RSM	DPM, RTD	RTD, Power measurements
		Hydraulic flocculator.	Full		$sk\text{-}\varepsilon$	RTD	Turbine meter velocity measurements
Craig et al., 2002	Fluent	Flow characteristics.	Pilot	ND	ND	ND	ND
Essemiani & de Traversay, 2002a	Fluent	Mixing efficiency.	Pilot	3D	$sk\text{-}\varepsilon$	None	RTD, Power No., Pumping No.
Essemiani & de Traversay, 2002b	Fluent	Comparison of mixer configurations.	Pilot	3D	$sk\text{-}\varepsilon$	None	RTD, Power No., Pumping No.
Haarhoff & van der Walt, 2001	Flo++	Hydraulic flocculator design optimization.	Full	3D	$sk\text{-}\varepsilon$	RTD	Turbine meter velocity measurements
Korpijarvi, Laine & Ahlstedt, 2000	CFX	G_L variations in jar tester.	Lab	3D	$sk\text{-}\varepsilon$, $RNG\ k\text{-}\varepsilon$, RSM	None	LDA, PIV

Table 5 (Continued)

Author	Code	Aim	Scale	Dim	Turb. Model	Extra Model	Validation method
Korpijarvi et al., 1999	CFX	Turbulence modelling and mesh density analysis jar tester.	Lab	3D	*sk-ε, RNG k-ε, LRN k-ε, RSM*	None	LDA, PIV
Lainé et al., 1999	Fluent	Flow characteristics to determine cause of underperformance.	Full	2D	*RNG k-ε*	DPM	None
Nopens, 2007	Fluent	Coupling CFD and PBM in wastewater clarifier.	Full	2D	*ske*	PBM (QMOM)	None
Prat & Ducoste, 2007	Phoenics	Evaluation of Lagrangian and Eulerian approaches for simulating flocculation in stirred vessels.	Lab	3D	*ske*	Lagrangian, Eulerian, PBM	Experimental data

N/A – not applicable, ND – not discussed, ADV – acoustic Doppler velocimetry, LDV – laser Doppler velocimetry, LDA – laser Doppler anemometry, PIV – particle image velocimetry, RTD – residence time distribution, MFM – multi-fluid model.

Most commercially-available CFD software has an in-built discrete phase model which can be used to model the trajectories of individual particles within a flow via integration of the force balance on a particle in a Lagrangian reference frame. Equating particle inertia with the forces acting on it, and applying a Cartesian co-ordinate system, yields:

$$\frac{du_p}{dt} = F_D(u - u_p) + \frac{g_x(\rho_p - \rho)}{\rho} + F_x \tag{25}$$

where, u is the fluid velocity, u_p is the particle velocity, μ is the dynamic viscosity of the fluid, and ρ and ρ_p are the fluid and particle densities, respectively, $F_D(u - u_p)$ is the drag force per unit particle mass, and

$$F_D = \frac{18\mu}{\rho_p d_p{}^2} \cdot \frac{C_D \, \text{Re}}{24} \tag{26}$$

where d_p is the particle diameter, and Re is the relative Reynolds number, defined as:

$$\text{Re} = \frac{\rho d_p |u_p - u|}{\mu} \tag{27}$$

The drag coefficient, C_D, is defined as:

$$C_D = \alpha_1 + \frac{\alpha_2}{\text{Re}} + \frac{\alpha_3}{\text{Re}^2} \tag{28}$$

where α_n are constants that apply to smooth spherical particles over several ranges of *Re* given by Morsi and Alexander (1972) (α_n values are shown in Appendix 2).

The term F_x in Eq. (25) relates to additional forces in the particle force balance that are relevant only under special circumstances; for example, forces on particles that arise due to the rotation of the reference frame. Considering rotation about the *z* axis, the forces on the particles in the *x* and *y* directions may be expressed as:

$$\left(1 - \frac{\rho}{\rho_p}\right)\Omega^2 x + 2\Omega\left(u_{y,p} - \frac{\rho}{\rho_p}u_y\right) \tag{29}$$

where $u_{y,p}$ and u_y are the particle and fluid velocities in the *y* direction, and

$$\left(1 - \frac{\rho}{\rho_p}\right)\Omega^2 y + 2\Omega\left(u_{x,p} - \frac{\rho}{\rho_p}u_x\right) \tag{30}$$

where $u_{x,p}$ and u_x are the particle and fluid velocities in the *x* direction.

However, the work of Morsi and Alexander (1972) was predicated on the assumption that particles are spherical, whereas flocs are irregularly-shaped,

mass fractal aggregates—i.e. they demonstrate self-similarity irrespective of scale and demonstrate a power law relationship between mass (or volume) and length, such that:

$$M \, \alpha \, L^{d_f} \tag{31}$$

where d_f is a non-integer mass fractal dimension. A low fractal dimension (<2.0) indicates an open structure, whereas a higher fractal dimension indicates a more compact structure. (For regular, three-dimensional objects, $d_f = 3.0$).

This fractal nature has some very important consequences on floc settlement and transport and the modelling thereof. For example, as floc size increases, the density decreases (Tambo and Watanabe, 1979), with the floc effective density represented by

$$\rho_E = B \cdot a^{-y} \tag{32}$$

where a is floc size and B and y are constants.

The effective density is proportional to the volume fraction of solid in the floc, such that

$$\rho_E = \phi_s(\rho_p - \rho) \tag{33}$$

and hence y is related to d_f via

$$d_f = 3 - y \tag{34}$$

Furthermore, because flocs are not spherical, the drag coefficient expression must be amended. Assuming the sphericity of flocs to be approximately 0.8, at low Reynolds numbers, Tambo and Watanabe (1979) suggested that

$$C_D \approx 45/\text{Re} \tag{35}$$

i.e. almost twice the value predicted via Stokes' law ($= 24/\text{Re}$).

Whilst this deviation from sphericity may be easily addressed via a simple adjustment to Eq. (28), the porosity of flocs (and hence the possibility of flow through the floc itself) poses additional modelling challenges. The net effect of porosity is that a floc will experience reduced drag compared to an impermeable sphere of the same size and density. This effect becomes significant for more open flocs with low fractal dimensions ($d_f < 2.0$), settling faster than solids of the same size and density.

However, the Lagrangian particle models treat all particles as point masses, and therefore cannot consider the effect of porosity directly. One means of addressing this is to assume that the porosity has an effect on the drag forces and consequently amend the drag coefficient accordingly. However, the means by which the information required to do this with any degree of

accuracy is unclear. This also involves further amendment of a coefficient to which adjustment has already been made to accommodate deviation from sphericity. This clearly adds an additional degree of uncertainty into the modelling process.

3.8 Population balance modelling (PBM)

Referring back to the modelling work undertaken on water treatment flocculation, it can be seen that much work in the water treatment field has addressed flow patterns. However, it is not just the hydrodynamic behaviour of flocculators which is of interest, but the agglomeration, growth and breakage processes are of great significance also. Multiphase models which incorporate a particle size distribution (PSD), such as those found in a flocculator, require a population balance model (PBM) to describe particle population changes. Several solution methods exist, including, inter alia, the discrete, class size method (Hounslow, Ryall and Marshall, 1998), the standard method of moments (SMM) (Randolph and Larson, 1971), and the quadrature method of moments (QMOM) (Marchisio, Vigil and Fox, 2003). A full description of each is outside the scope of this paper and only brief comments on each are made.

The discrete method requires the particle population to be discretised into a finite number of size bins and is based on the representation of the PSD in terms of those bins. This method has the advantage that the PSD is calculated directly; however, the bins must be defined from the outset and a large number may be required. Further, the coupling of CFD and PSD models requires the incorporation of transport equations in each bin, making the process computationally expensive.

Unlike the discrete method, moment methods simulate statistical information about the PSD, rather than deriving an accurate description of the PSD. With the SMM, the population balance equation is transformed into a set of transport equations for moments of the distribution which, for lower-order moments, are relatively easy to solve. No prior assumptions are made with regard to the size distribution and the moment equations are closed (involving only functions of the moments themselves). However, this latter point prevents particle aggregation and breakage being written as functions of moments, thus meaning that the method is only applicable in situations of constant aggregation, size independent, and growth. For the simulation of flocculation in water treatment, these are significant limitations. However, these limitations can be overcome via use of the QMOM. The QMOM offers reduced computational expense compared to the discrete model, but it differs from the SMM by replacing the exact closure with an approximate closure, requiring only a small number of scalar equations to track population moments (McGraw, 1997). The reduced computational cost of the moment methods means that they can be combined with CFD calculations such that the effects of local (rather than global average) flow field characteristics can be considered.

Whilst the development of PBM techniques has advanced, the coupling of PBMs with CFD remains in its infancy, particularly in water treatment applications with most (but not all) work being undertaken using wastewater. Prat and Ducoste (2007) considered the evolution of flocs using the QMOM and used CFD to solve the turbulent flow field within a 28 litre stirred vessel with clay particles. Whilst the results provide proof of concept for the decoupling of fluid flow and flocculation dynamics in the Lagrangian/QMOM approach, they do not provide information regarding the growth and strength of flocs in specific water treatment applications. Other recent work includes that of Nopens (2007) (CFD and QMOM-based PBM in wastewater clarifier) and Feng and Li (2008) (theoretical PBM approach, encapsulating internal body forces and fluid shear stress). A detailed review of all recent PBM work is outside the scope of this paper; the interested reader is referred to Hounslow, Ryall and Marshall (1988), Nopens and Vanrolleghem (2006) and Coufort et al. (2007). It is the work of Nopens which would appear to have advanced the application of CFD and PBM modelling to the greatest extent thus far. However, it is clear from the literature that there has been no work undertaken on raw waters abstracted from WTW at either lab or full scale. Consequently, there remains the need to simulate accurately realistic water treatment flocculation processes at both laboratory scale using raw water samples taken from WTW, and also at full scale.

4. CONCLUSIONS

The use and application of CFD within water treatment has expanded significantly over the period 1995–2008. Examples of the technique's application can be found for most unit processes, from the storage of raw water, through detailed and technical water treatment processes, to chemical disinfection. Model complexity varies from application of two-equation turbulence

models to straightforward geometries, to the use of the RSM and sliding mesh technique, coupled with Eulerian or Lagrangian discrete phase model, in mixing scenarios.

There are several published examples of where CFD has been applied to model bulk flow patterns in the complex, swirling flow found in mechanically mixed flocculators. However, there are few examples which extend the analysis to consider floc trajectory or fate. Lagrangian techniques are available, but are somewhat limited by the fractal nature of flocs and, in particular, the impacts of density and porosity on drag force and settlement characteristics.

CFD has been used effectively to demonstrate the limitations of the average velocity gradient approach to classifying flocculators.

Whilst a Volume of Fluid model can be used to indicate the likelihood of vortex formation, it is ill-equipped to deal with the bubble formation arising from the breaking of the air/water interface when air passes through grid cells where large momentum sources exist and so should not be used to predict post vortex formation flow conditions.

There remain several areas which require further study to facilitate their accurate representation using CFD. In particular, the robust coupling of population balance modelling for flocculation processes with CFD models for water treatment processes remains a key challenge. Progress has been made in wastewater flocculation; however, there remains the need to simulate accurately realistic water treatment flocculation processes at both laboratory scale using raw water samples taken from WTW, and also at full scale.

ACKNOWLEDGEMENTS

REFERENCES

1. Bakker A, LaRoche RD, Wang MH, Calabrese RV (2000). "Sliding Mesh Simulation of Laminar Flow in Stirred Reactors." In *The Online CFM Book*, http://www.bakker.org/cfm. (Accessed 7th November 2006).

2. Biggs CA, Lant PA (2000). Activated sludge flocculation: On-line determination of floc size and the effect of shear. *Water Research* 34:2542–2550.

3. Boller M, Blaser S (1998). Particles under stress. *Water Science and Technology* 37(10):9–29.

4. Bouyer D, Coufort C, Liné A, Do-Quang Z (2005). Experimental analysis of floc size distributions in a 1-L jar under different hydrodynamics and physico-chemical conditions. *J. Colloid Interface Sci*. 292:413–428.

5. Bridgeman J, Jefferson B, Parsons SA (2007). The development and use of CFD models for water treatment processes. *CC2007: The Eleventh International Conference on Civil, Structural and Environmental Engineering Computing*, St. Julians, Malta, 18–21 September.

6. Bridgeman J, Jefferson B, Parsons SA (2008). Assessing floc strength using CFD to improve organics removal. *Chemical Engineering Research and Design* 86(8):941–950.

7. Camp TR, Stein PC (1943). Velocity gradients and internal work in fluid motion. *Journal of the Boston Society of Civil Engineers* 30(4):219–237.

8. Clark MM (1985). Critique of Camp and Stein's RMS velocity gradient. *J. Environmental Engineering* 111(6):741–754.

9. Cleasby JL (1984). Is velocity gradient a valid turbulent flocculation parameter? *J. Environmental Engineering* 110(5):875–897.

10. Coufort C, Bouyer D, Liné A (2005). Flocculation related to local hydrodynamics in a Taylor-Couette reactor and in a jar. *Chemical Engineering Science* 60:2179–2192.

11. Coufort C, Bouyer D, Liné A, Haut B (2007). Modelling of flocculation using a population balance equation. *Chemical Engineering and Processing* 46:1264–1273.

12. Craig K, de Traversay C, Bowen B, Essemiani K, Levecq C, Naylor R (2002). Hydraulic study and optimisation of water treatment processes using numerical simulation. *Water Science and Technology: Water Supply* 2(5–6):135–142.

13. Crittenden JC, Trussell RR, Hand DW, Howe KJ, Tchobanoglous G (2005). *Water Treatment: Principles and Design*. 2nd Ed., John Wiley and Son.

14. Ducoste JJ, Clark MM (1999). Turbulence in flocculation: comparison of measurements and CFD simulations. *AIChE J.* 45(2):432–436.

15. Essemiani K, de Traversay C (2002a). Optimisation of the flocculation process using computational fluid dynamics. *Chemical Water and Wastewater Treatment VII, Proceedings of the 10th Gothenburg Symposium*. Ed. Hahn HH, Hoffmann E, Odegaard H, IWA Publishing.

16. Essemiani K, de Traversay C (2002b). Optimum design of coagulation / flocculation vessels. *WQTC 2002 conference*, Seattle, USA.

17. Feng X, Li XY (2008). Modelling the kinetics of aggregate breakage using improved breakage kernel. *Wat. Sci. Tech.* 57(1):151–157.

18. Fluent Inc. (2005). *Fluent 6 Users' Guide*.

19. Freitas CJ (1995). Perspective: Selected benchmarks from commercial CFD codes. *J. Fluids Engineering* 117:210–218.

20. Graber SD (1994). A critical review of the use of the *G*-value (RMS velocity gradient) in environmental engineering. *Dev. Theor. Appl. Mech.* 17:533–556.

21. Haarhoff J, van der Walt JJ (2001). Towards optimal design parameters for around-the-end hydraulic flocculators. *J. Water Supply: Research and Technology-AQUA* 50(3):149–159.

22. Haque JN, Mahmud T, Roberts KJ (2006). Modelling flows with free-surface in unbaffled agitated channels. *Ind. Eng. Chem. Res.* 45:2881–2891.

23. Hounslow M, Ryall R, Marshall V (1988). A discretized population balance for nucleation, growth, and aggregation. *AIChE. J.* 34(11):1821–1832.

24. Iaccarino G (2000). Prediction of the turbulent flow in a diffuser with commercial CFD codes. *Centre for Turbulence Research Annual Research Briefs*, 271–278.

25. Jones SC (1999). *Static mixers for water treatment. A computational fluid dynamics model*. PhD Thesis, Georgia Institute of Technology.

26. Korpijarvi J, Ahlstedt H, Saarenrinne P, Renanen J (1999). Modelling of flow field in the mini-flocculator. *IChemE Symposium Series No. 146, Fluid Mixing 6*. Ed. Benkreira H, 361–372.

27. Korpijarvi J, Laine E, Ahlstedt H (2000). Using CFD in the study of mixing in coagulation and flocculation. *Chemical Water and Wastewater Treatment VI, Proceedings of the 9th Gothenburg Symposium*. Ed. Hahn HH, Hoffmann E, Odegaard H, Springer, 89–99.

28. Kusters K, Wijers J, Thoenes D (1997). Aggregation kinetics of small particles in agitated vessels. *Chem. Eng. Sci.* 52(1)107–121.

29. Lainé S, Phan L, Pellarin P, Robert P (1999). Operating diagnostics on a flocculator-settling tank using FLUENT CFD software. *Water Science and Technology* 39(4):155–162.

30. Launder BE, Spalding DB (1974). *Lectures in Mathematical Models of Turbulence*. Academic Press, London, UK.

31. Luo C (1997). *Distribution of velocities and velocity gradients in mixing and flocculation vessels: comparison between LDV data and CFD predictions*. PhD Thesis, New Jersey Institute of Technology.

32. Luo JY, Issa RI, Gosman AD (1994). Prediction of impeller induced flows in mixing vessels using multiple frames of reference. *IChemE Symposium Series No. 136*, 549–556.

33. Marchisio D, Vigil R, Fox R (2003). Quadrature method of moments for aggregation-breakage processes. *J. Col. Int. Sci.* 258(2):322–334.

34. Marshall EM, Bakker A (2004). "Computational Fluid Mixing." In *Handbook of Industrial Mixing: Science and Practice*. Ed. Paul EL, Atiemo-Obeng VA, Kresta SM, 257–343.

35. McGraw R (1997). Description of aerosol dynamics by the quadrature method of moments. *Aero. Sci. and Tech.* 27(2):255–265.

36. Menter FR (2003). Turbulence modelling for turbomachinery. *QNET-CFD Network Newsletter* 2(3):10–13.

37. Mikkelsen L (2001). The shear sensitivity of activated sludge: relations to filterability, rheology and surface chemistry. *Coll. Surf. A* 182:1–14.

38. Morsi SA, Alexander A (1972). An investigation of particle trajectories in two-phase flow systems. *J. Fluid Mechanics* 55(2):193–208.

39. Ng K, Borrett NA, Yianneskis M (1999). On the distribution of turbulence energy dissipation in stirred vessels. *IChemE Symposium Series No. 146, Fluid Mixing 6*. Ed. Benkreira H, 69–80.

40. Nopens I (2007). Improved prediction of effluent suspended solids in clarifiers through

integration of a population balance model and a CFD model. *PS-IWA 2007: Particle Separation*, Toulouse.

41. Nopens I, Vanrolleghem PA (2006). Comparison of discretization methods to solve a population balance model of activated sludge flocculation including aggregation and breakage. *Mathematical and Computer Modelling of Dynamical Systems* 12(5):441–454.

42. Paul EL, Atiemo-Obeng VA, Kresta SM (2004). *Handbook of Industrial Mixing: Science and Practice*. Wiley-Interscience.

43. Prat OP, Ducoste JJ (2007). Simulation of flocculation in stirred vessels—Lagrangian versus Eulerian. *Chem Eng Res. and Des.* 85(A2):207–219.

44. Randolf AD, Larson MA (1971). *Theory of Particulate Processes*. Academic Press, New York.

45. Rodi W (1993). *Turbulence Models and Their Application in Hydraulics*. 3rd Ed., IAHR.

46. Tambo N, Wanatabe Y (1979). Physical aspects of flocculation—I The flocculation density function and aluminium floc. *Water Research* 13:409–419.

47. Thomas, DG (1964). Turbulent disruption of flocs in small particle size suspensions. *J. AIChE* 19(4):517–523.

48. Van der Walt JJ (1998). The application of computational fluid dynamics in the calculation of local G values in hydraulic flocculators. *Proceedings of the Biennial Conference of the Water Institute of Southern Africa*, 1998, Cape Town, South Africa. (Available at: http://www.ewisa.co.za/ literature/files/1998%20-%2079.pdf, accessed February 2009.)

49. Versteeg HK, Malalasekera W (1995). *An Introduction to Computational Fluid Dynamics. The Finite Volume Method*. Prentice Hall.

50. Yeung AKC, Gibbs A, Pelton RP (1997). Effect of Shear on the Strength of Polymer-Induced Flocs. *Journal of Colloid and Interface Science* 196:113–115.

APPENDIX 1

Standard k-ε Model

$$\frac{\partial}{\partial t}(\rho k) + \frac{\partial}{\partial x_i}(\rho k u_i) = \frac{\partial}{\partial x_j}\left[\left(\mu + \frac{\mu_t}{\sigma_k}\right)\frac{\partial k}{\partial x_j}\right] + G_k - \rho\varepsilon \tag{A1}$$

$$\frac{\partial}{\partial t}(\rho\varepsilon) + \frac{\partial}{\partial x_i}(\rho\varepsilon u_i) = \frac{\partial}{\partial x_j}\left[\left(\mu + \frac{\mu_t}{\sigma_\varepsilon}\right)\frac{\partial \varepsilon}{\partial x_j}\right] + C_1\frac{\varepsilon}{k}G_k - C_2\rho\frac{\varepsilon^2}{k} \tag{A2}$$

where the turbulent viscosity, μ_t, is calculated according to

$$\mu_t = \rho C_\mu \frac{k^2}{\varepsilon} \tag{A3}$$

and the generation of turbulence kinetic energy due to mean velocity gradients, G_k,

$$G_k = \mu_t\left(\frac{\partial u_i}{\partial x_j} + \frac{\partial u_j}{\partial x_i}\right)\frac{\partial u_j}{\partial x_i} \tag{A4}$$

σ_k and σ_ε are the effective Prandtl numbers for k and ε, respectively.

The empirical model constant values are generally accepted as $C_\mu = 0.09$, $C_1 = 1.44$, $C_2 = 1.92$, $\sigma_k = 1.0$ and $\sigma_\varepsilon = 1.3$.

Renormalized Group (RNG) k-ε Model

$$\frac{\partial}{\partial t}(\rho k) + \frac{\partial}{\partial x_i}(\rho k u_i) = \frac{\partial}{\partial x_j}\left[\left(\alpha_k\mu_{eff}\right)\frac{\partial k}{\partial x_j}\right] + G_k - \rho\varepsilon \tag{A5}$$

$$\frac{\partial}{\partial t}(\rho\varepsilon) + \frac{\partial}{\partial x_i}(\rho\varepsilon u_i) = \frac{\partial}{\partial x_j}\left[(\alpha_\varepsilon \mu_{eff})\frac{\partial\varepsilon}{\partial x_j}\right] + C_{1\varepsilon}\frac{\varepsilon}{k}G_k - C_2\rho\frac{\varepsilon^2}{k} - R_\varepsilon \tag{A6}$$

$$\mu_{eff} = \mu + \mu_t$$

α_k and α_ε are the inverse effective Prandtl numbers for k and ε, respectively.

Realizable k-ε Model

$$\frac{\partial}{\partial t}(\rho k) + \frac{\partial}{\partial x_j}(\rho k u_j) = \frac{\partial}{\partial x_j}\left[\left(\mu + \frac{\mu_t}{\sigma_k}\right)\frac{\partial k}{\partial x_j}\right] + G_k - \rho\varepsilon + S_k \tag{A7}$$

$$\frac{\partial}{\partial t}(\rho\varepsilon) + \frac{\partial}{\partial x_j}(\rho\varepsilon u_j) = \frac{\partial}{\partial x_j}\left[\left(\mu + \frac{\mu_t}{\sigma_\varepsilon}\right)\frac{\partial\varepsilon}{\partial x_j}\right] + \rho C_1 S_\varepsilon - \rho C_2\frac{\varepsilon^2}{k + \sqrt{\nu\varepsilon}} + C_{1\varepsilon}\frac{\varepsilon}{k}C_3 G_b + S_\varepsilon \tag{A8}$$

C_2 is a constant. σ_k and σ_ε are the turbulent Prandtl numbers for k and ε, respectively. S_k and S_ε are user-defined source terms. The empirical model constant values are generally accepted as $C_{1\varepsilon} = 1.44$, $C_1 = \max\left[0.43, \frac{\eta}{\eta+5}\right]$, $C_2 = 1.9$, $\sigma_k = 1.0$ and $\sigma_\varepsilon = 1.2$.

k-ω Model

$$\frac{\partial}{\partial t}(\rho k) + \frac{\partial}{\partial x_i}(\rho k u_i) = \frac{\partial}{\partial x_j}\left[\Gamma_k\frac{\partial k}{\partial x_j}\right] + G_k - Y_k + S_k \tag{A9}$$

$$\frac{\partial}{\partial t}(\rho\omega) + \frac{\partial}{\partial x_i}(\rho\omega u_i) = \frac{\partial}{\partial x_j}\left[\Gamma_\omega\frac{\partial\omega}{\partial x_j}\right] + G_\omega - Y_\omega + S_\omega \tag{A10}$$

Γ_k and Γ_ω represent the effective diffusivity of k and ω respectively

$$\Gamma_k = \mu + \frac{\mu_t}{\sigma_k} \tag{A11}$$

$$\Gamma_\omega = \mu + \frac{\mu_t}{\sigma_\omega} \tag{A12}$$

G_k represents the generation of turbulence kinetic energy due to mean velocity gradients. G_ω represents the generation of ω. Y_k and Y_ω represent the dissipation of k and ω due to turbulence. S_k and S_ε are user-defined source terms.

SST k-ω Model

$$\frac{\partial}{\partial t}(\rho k) + \frac{\partial}{\partial x_i}(\rho k u_i) = \frac{\partial}{\partial x_j}\left[\Gamma_k\frac{\partial k}{\partial x_j}\right] + G_k - Y_k + S_k \tag{A13}$$

$$\frac{\partial}{\partial t}(\rho\omega) + \frac{\partial}{\partial x_i}(\rho\omega u_i) = \frac{\partial}{\partial x_j}\left[\Gamma_\omega\frac{\partial\omega}{\partial x_j}\right] + G_\omega - Y_\omega + D_\omega + S_\omega \tag{A14}$$

D_ω represents the cross-diffusion term.

Reynolds Stress Model

Considering an incompressible flow without body forces and ignoring transport due to rotation, the exact equation for the transport of the Reynolds stresses ($= \rho \overline{u_i \, u_j}$) is

$$\frac{\partial}{\partial t}(\rho \overline{u_i' u_j'}) + \frac{\partial}{\partial x_k}(\rho u_k \overline{u_i' u_j'}) = -\frac{\partial}{\partial x_k}\left[\rho \overline{u_i' u_j' u_k'} + \overline{p(\delta_{kj} u_i' + \delta_{ik} u_j')}\right] + \frac{\partial}{\partial x_k}\left[\mu \frac{\partial}{\partial x_k}(\overline{u_i' u_j'})\right]$$

local time   convection   turbulent diffusion   molecular diffusion
derivative

$$-\left(\rho \overline{u_i' u_k'} \frac{\partial u_j}{\partial x_k} + \overline{u_j' u_k'} \frac{\partial u_i}{\partial x_k}\right) + \overline{p\left(\frac{\partial u_i'}{\partial x_j} + \frac{\partial u_j'}{\partial x_i}\right)} - 2\mu\left(\frac{\partial u_i'}{\partial x_k} \frac{\partial u_j'}{\partial x_k}\right)$$

stress production   pressure strain   dissipation

APPENDIX 2

Drag coefficient parameters (from Morsi and Alexander, 1972):

$$C_D = \alpha_1 + \frac{\alpha_2}{\text{Re}} + \frac{\alpha_3}{\text{Re}^2}$$

Re	α_1	α_2	α_3
< 0.1	0	24	0
0.1–1.0	3.69	22.73	0.0903
1.0–10	1.222	29.1667	-3.8889
10–100	0.6167	46.5	-116.67
100–1,000	0.3644	98.33	-2778
1,000–5,000	0.357	148.62	-4.75×10^4
5,000–10,000	0.46	-490.546	57.87×10^4
10,000–50,000	0.5191	-1662.5	5.4167×10^6